J Mol Model (2012) 18:3181–3197
DOI 10.1007/s00894-011-1326-7

ORIGINAL PAPER

Inter- versus intra-molecular cyclization of tripeptides containing tetrahydrofuran amino acids: a density functional theory study on kinetic control

N. V. Suresh Kumar · U. Deva Priyakumar · Harjinder Singh · Saumya Roy · Tushar Kanti Chakraborty

Received: 4 October 2011 / Accepted: 2 December 2011 / Published online: 12 January 2012

Abstract Density functional B3LYP method was used to investigate the preference of intra- and inter-molecular cyclizations of linear tripeptides containing tetrahydrofuran amino acids. Two distinct model pathways were conceived for the cyclization reaction, and all possible transition states and intermediates were located. Analysis of the energetics indicate intermolecular cyclization being favored by both thermodynamic and kinetic control. Geometric and NBO analyses were performed to explain the trends obtained along both the reaction pathways. Conceptual density functional theory-based reactive indices also show that reaction pathways leading to intermolecular cyclization of the tripeptides are relatively more facile compared to intramolecular cyclization.

Keywords Peptides · Cyclization · Planarity · DFT · NBO

Introduction

Peptides and peptidomimetics have attracted great interest for their potential in a wide range of applications from therapeutics to nanomaterials [1, 2]. Particularly, the cyclic variants, with their additional conformational restraints and stability towards proteases, are of greater significance than their linear counterparts. Along with several naturally occurring bioactive macrocyclic peptides [3–15] like vancomycin [16], cyclosporine [17], gramicidin S [18], various designed cyclic peptides [19], RGD-peptides [20], stapled peptides [21] and peptidomimetics containing β-amino acids [22], γ-amino acids [23], sugar amino acids [24], alternating sequence of D- and L- amino acids [25], and heterocyclic backbones [26, 27] have also shown promising therapeutic effectiveness and their number is increasing very rapidly [28, 29]. In addition, the ring size of a cyclic peptide has a remarkable effect on activity during interaction with the lipid bi-layer of cellular membranes [30]. Naturally, syntheses of symmetrical and unsymmetrical cyclic peptides with different ring sizes would be a valuable approach in drug discovery research. However, despite several strategies involving wide ranging coupling reagents, to cyclize a linear peptide into its macrocyclic version is always challenging. Often it leads to either poor yield of the desired product or higher cyclooligomeric or polymeric undesired products. The preformed conformation of the linear peptide and the individual amino acid components are the deciding factors for the success of the macrocyclization. In addition, iterative coupling of amino acid constituents to synthesize the linear peptide leads to several unwanted problems, such as racemization or side reactions. Cyclooligomerization [31] is one of the best step-economical strategies for the synthesis of symmetrical cyclic peptides from linear subunits in a convergent manner. However, the control of ring size during cyclooligomerization necessarily depends on the constituents of the subunits, their 3D structures, and the energies of the precursors and products. The reactivity of the functional groups under both thermodynamic and kinetic conditions could also have a profound impacts on the

Electronic supplementary material The online version of this article (doi:10.1007/s00894-011-1326-7) contains supplementary material, which is available to authorized users.

N. V. S. Kumar · U. D. Priyakumar · H. Singh (✉)
Center for Computational Natural Sciences and Bioinformatics,
International Institute of Information Technology,
Hyderabad 500 032, India
e-mail: laltu@iiit.ac.in

S. Roy · T. K. Chakraborty
Central Drug Research Institute, CSIR,
Lucknow 226 001, India

selective formation of the resultant ring size of the products. In this regard, theoretical studies on the mode of cyclization of smaller subunits with suitably oriented reactive termini available for coupling with other reactive partners assume great significance for accurate prediction of the outcome of such cyclooligomerization reactions [32–38]. We have long used furanoid- and pyranoid-based sugar amino acids [39, 40] as multifunctional templates to synthesize linear and cyclic hetero and homooligomeric libraries.

Very recently, our designed cyclodimeric amphiphilic peptides [41, 42] were shown to have antimicrobial activity against various cells by destroying the cellular membrane. In order to synthesize these cyclic dimeric peptidomimetics, we used two different linear peptides: TAA1 and TAA2 (see Fig. 1). Cyclodimerization was performed for each peptide in a single step using pentafluorophenyl diphenyl phosphinate (FDPP) [43] as a cyclizing reagent in acetonitrile solvent under dilute conditions. Gratifyingly, the only product isolated was the intermolecularly cyclodimerized molecule, with no trace of any intramolecularly cyclized product [41]. Extensive NMR techniques (NOESY), classical molecular dynamics (MD), circular dichroism (CD) and mass spectrometric analyses proved this phenomenon. This led us to investigate the stabilities of the cyclic C_2 symmetric hexapeptides and cyclic tripeptides based on density functional theory (DFT) [44] calculations, and we found that cyclic hexapeptide products are thermodynamically more stable than cyclic tripeptides [45].

In the present study, we report the role of kinetic control on the formation of cyclic hexapeptides vs tripeptides by modeling the transition states and intermediates for the two cyclization reactions. For this purpose, we looked into various mechanisms of peptide bond formation available in the literature. For example, in realistic situations, a reaction mechanism proposed for peptide bond formation uses FDPP as a catalyst [46, 47]. The mechanism is shown in Fig. 2a. Peptide coupling in solution requires activation of the acid, e.g., via an intermediate like C(=O)OPfp (OPfp: pentafluorophenol ester). The amine then attacks the activated acid, causing the OX anion to leave in a kind of nucleophilic displacement (Fig. 2a). On the other hand, the uncatalyzed mechanisms investigated by Oie et al. [48] and Jensen et al. [49], are straightforward (Fig. 2b). The mechanisms of reactions involving formation of a peptide bond are associated with elimination of water molecule(s). The latter authors studied the mechanisms using two different models (Fig. 2b): (1) a stepwise pathway, where one of the hydrogen atoms of the $–NH_2$ group is shifted to the oxygen of C=O resulting in a diol intermediate; the second step involves the elimination of water forming the peptide bond; (2) a concerted pathway involving direct elimination of a water molecule, using the –OH from the carboxyl terminal and the –H of the amine group. The reaction mechanism for the reverse process, i.e., amide hydrolysis via concerted and stepwise mechanisms was also investigated by Krug et al. [50] and Antonczak et al. [51]. As the straightforward mechanisms require lower computational cost, geometries involved in reaction pathways for the cyclization reactions shown in Fig. 1 were modeled using these mechanisms in gas phase.

Schematic representations of the intra- and inter-molecular cyclization pathways, the corresponding transition states, intermediates and products are outlined in Figs. 3 and 4,

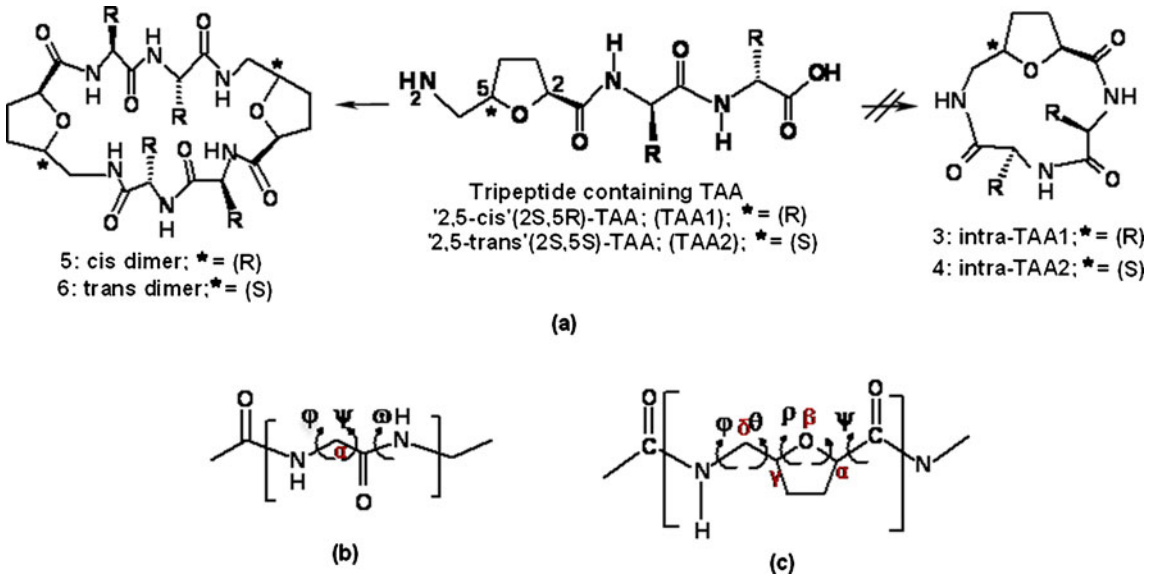

Fig. 1 **a** Reactions leading to formation of inter- and intra-molecularly cyclized products from TAA1 and TAA2. Conventional atom numbering is used here in the tetrahydrofuran ring to represent the chiral centers. **b** α-Peptide. **c** δ -Peptide formed by tetrahydrofuran amino acid

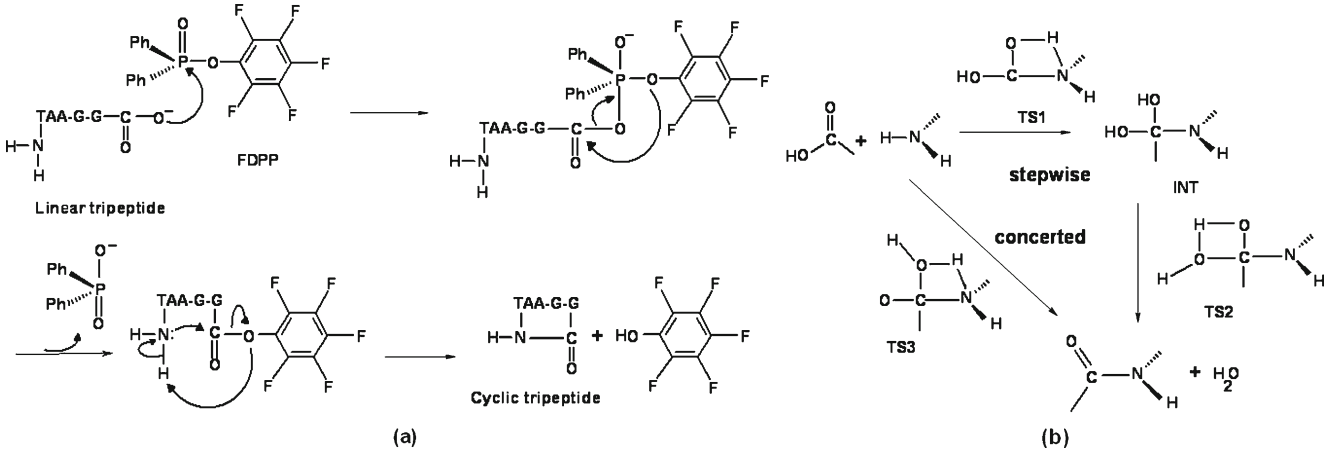

Fig. 2 **a**,**b** Mechanisms suggested in the literature for peptide bond formation. **a** A pathway with a catalyst pentafluorophenyl diphenyl phosphinate (FDPP). **b** The uncatalyzed stepwise and concerted pathways

respectively. As intermolecular cyclization involves formation of two peptide bonds, we investigated two routes of stepwise mechanism ('a' and 'b', see Fig. 4) for cyclodimerization reactions. In a stepwise mechanism, a diolic intermediate is obtained during formation of a peptide bond and a transient geometry immediately follows that transfers a proton from one of the –OH groups to another such that the water molecule gets detached and a linear hexapeptide is formed. In the stepwise-b mechanism, the diolic intermediate transfers a proton from NH_2 to the oxygen atom of C=O such that a cyclic compound associated with two diol groups is formed.

Studies that considered ionic intermediates and transition states as models have shown the necessity of micro solvation [52]. It is worth mentioning here that, in the present study, the complexity of the solvent-assisted reaction pathway was not addressed, and a more detailed future investigation with different possibilities for microsolvation is foreseen as faster technology becomes accessible.

Linear tripeptides, TAA1 and TAA2 are denoted as **1** and **2** respectively. Intra(inter)molecularly cyclized products obtained from **1** and **2**, are referred to as intra-TAA1, **3** (cisdimer, **5**), intra-TAA2, **4** (trans dimer, **6**), respectively, in the following. Wherever convenient, the cyclized products are referred to as 'intra product' and 'inter product', where further discrimination is not required. Notation for other geometries involved in the reactions is shown in Figs. 3 and 4. Reactions involving intra(inter)molecular cyclization of **1** and **2** are referred to as **1Cy(1Cy-di)** and **2Cy(2Cy-di)**, respectively.

Methodology

The coordinates of cis and trans dimers (Fig. 1) were available from NMR experiments [46]. The conformational space of each cyclized geometry was examined using the random search method of Sybyl7.2 [53], which explores the space by making random changes to select torsional angles followed by energy minimization [54]. We allowed for rotation about all N–C_α and C_α –C bonds of α-amino acid residues, and the N–C_δ bond of the δ -amino acid in case of both intra and inter products (Fig. 1). The random search parameters were set to default values with energy cutoff value of 10 kcal/mol, and

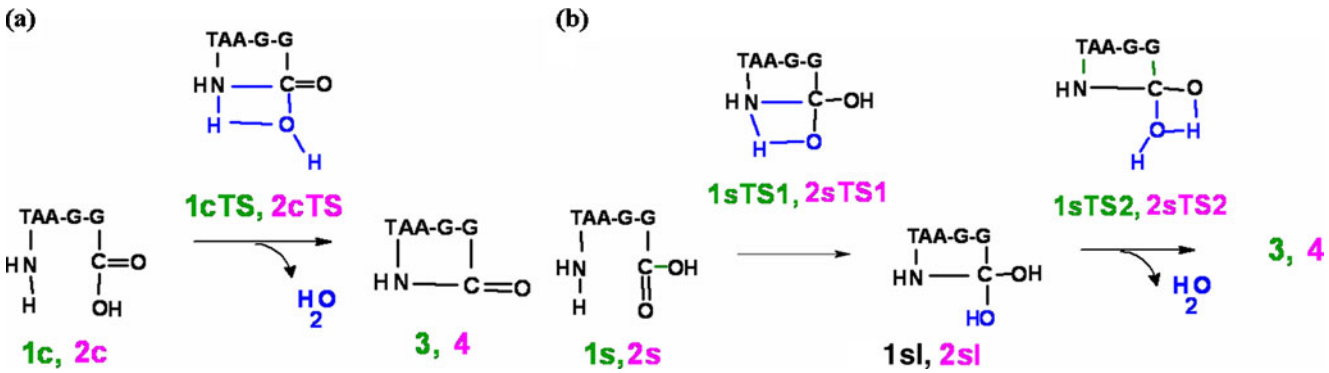

Fig. 3 Line drawings for structures in (**a**) concerted and (**b**) stepwise intramolecular cyclization reactions of TAA1 and TAA2. *1* TAA1, *2* TAA2, *s* stepwise, *c* concerted, *TS* Transition state, *TS1-2* Transition state 1-2, *I* Intermediate, *3* intra-TAA1, *4* intra-TAA2

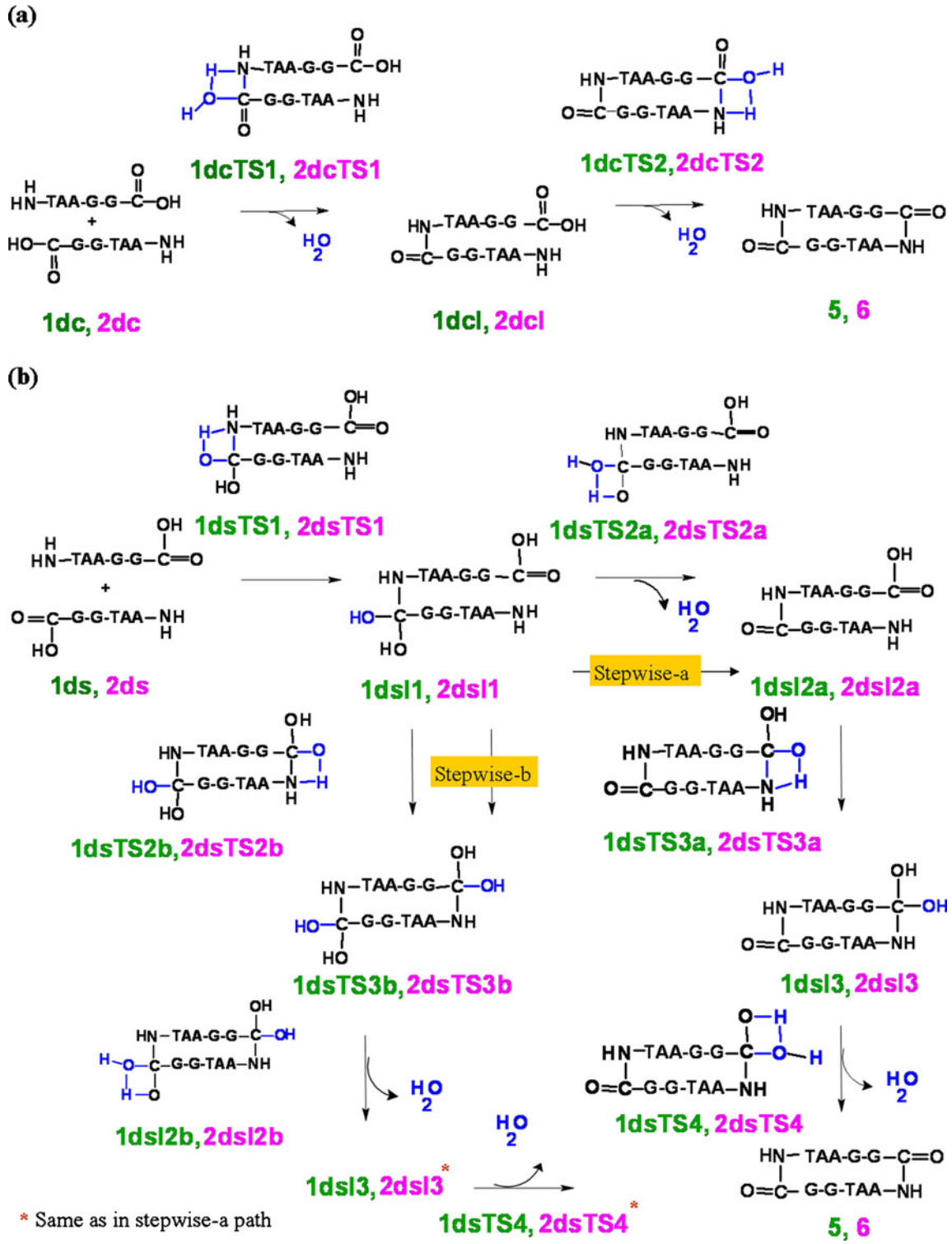

Fig. 4 Line drawings for structures in **a** concerted, **b** stepwise-a, -b intermolecular cyclization reactions of TAA1 and TAA2. Representation of symbols used in notation is as follows; *1* TAA1, *2* TAA2, *d* dimerization, *c* concerted, *s* stepwise, *TS1-2-3-4* Transition state 1-2-3-4, *I1* Intermediate 1, *I2a-3a* Intermediate 2 and 3 obtained in mechanism stepwise-a, *I2b-3b* Intermediate 2 and 3 obtained in mechanism stepwise-b, *I3* Intermediate 3, *5* cis dimer, *6* trans dimer

with the chirality check turned on. The search yielded five initial conformations of the cis dimer, 36 of intra-TAA1, 7 of the trans dimer and 12 of intra-TAA2. All conformers, including geometries obtained from NMR experiment, were subjected to single point energy calculations at B3LYP [55–57] /6-31G(d,p) [58] level of density functional theory

(DFT). The lowest energy structures obtained from QM calculations were further subjected to optimization at the B3LYP /6-31G(d,p) level of theory.

The products are expected to be conformationally more rigid compared to the reactants. The number of possible conformers for the reactants, cyclic intermediates and transition states are relatively larger. Thus, modeling of these species was based on the minimum energy structures of the products. For example, the transition state, **1dsTS4** was obtained by keeping a water molecule close to the carbonyl group of most stable conformer of **5**, followed by transition state optimization. Similarly, **1dsI3** was obtained by elongating and shortening selected bonds in **1dsTS4** followed by energy minimization, and so on. The geometries obtained by this process are expected to be consistent models for comparison with each other.

All the reactants, transition states and intermediates were optimized at the B3LYP/6-31G(d,p) level of theory using the default cutoff for convergence implemented in the Gaussian03 [62] program. Hessian calculations were carried out on all optimized geometries at the same level of theory in order to confirm that the structures of reactants, intermediates and products lie at minima (all real frequencies) and transition states at first order saddle point (one imaginary frequency). Visual analysis of nuclear motion in the TS confirms the mechanism suggested in Figs. 3 and 4. Displacements of groups H, O–H (in water) and C(–N) in **1sTS2** and **1cTS** in modes of vibration with imaginary frequency provide insights into reaction coordinates [59–61]. All the relative energies (ΔE, E: zero point corrected electronic energy) and free energies (ΔG) presented in this paper were calculated with respect to the most stable conformer of the reactants. A breakdown of change in free energy in terms of enthalpy and entropy change was employed to provide insights into the role of thermodynamic parameters in favorable and unfavorable cyclization reactions. The Eyring equation [63],

$$k = \frac{k_B T}{h} exp \frac{\Delta G^{\ddagger}}{RT} \tag{1}$$

where k_B is the Boltzmann constant, T is the absolute temperature and $\Delta G^{\ddagger}$ is the free energy of activation, was used to determine the rate determining steps of intermolecular cyclization reactions. The predicted kinetic constants are based on conventional transition state theory. In principle, the variational transition state theory should give more reliable results. A recent study by Chiodo et al. [64] on the two procedures has shown that the two theories give similar results.

Single point energy calculations were carried out using an array of basis sets, namely, 6-311G(d,p), 6-311+G(d,p), 6-311++G(d,p), cc-pVDZ, aug-cc-pVDZ and cc-pVTZ in order to estimate the dependence of energies on the quality of basis set used. Additionally, calculations were also carried out at MP2/6-31G(d,p) level of ab initio theory for the same systems. Effects of electron correlation on reaction energies of the species were studied by comparing electronic energies obtained at the MP2 and B3LYP levels of theory. It should be noted that the B3LYP calculations presented here may not suffice for larger systems where stacking may be possible. However, the systems considered here are stabilized mostly by hydrogen bonding; the missing dispersion component and error due to basis set superposition (BSSE) are expected to approximately compensate each other [65].

Recent studies on nonplanarity of trans peptide bonds [66–72] were used to analyze torsional rotation around the bond during intra and intermolecular cyclization of the tripeptides. Intramolecular hydrogen bonding interactions, A…H–D in all geometries obtained in a mechanistic study of the reactions that fall within the criteria [45]: 1.5 Å ≤ A…D distance ≤ 3.2 Å, and 120° ≤ A…H-D bond angle ≤ 180° were determined. Structures analogous to secondary folding patterns, such as turns, and their association with H-bonds were characterized by torsion angles in cyclized product geometries. Formation of 10 and 13 membered H-bonded cycles across the THF ring was analyzed in terms of orientation of substitutions at the 2, 5 positions of the ring. The orientation of the ring substitutions is 'equatorial' (referred to as eq) if $90 \leq |\zeta / \rho| \leq 120$ and is 'axial' (referred to as ax) if $120 \leq |\zeta / \rho| \leq 180$ [32, 73]. Torsion angles, ζ and ρ were defined according to conventional definitions of peptide torsion angles and shown in Fig. 1.

The natural bond orbital (NBO) [74] program was used to evaluate stabilization energies of hydrogen bonding interactions. Correlation between geometrical parameters of H-bond, stabilization energy, $E^{(2)}$, and occupancy on σ^*_{NH} was investigated.

Chemical hardness and electric polarizability profiles were also studied to gain additional insights into correspondence between variations of hardness, polarizability and energetics of species involved. Qualitative concepts, molecular hardness (η), and chemical potential (μ), which is the negative of electronegativity (χ), were calculated using the approximate Eqs. 2 and 3 [75]:

$$\eta = \frac{1}{2}(\varepsilon_L - \varepsilon_H) \tag{2}$$

and

$$\mu = -\chi = \frac{1}{2}(\varepsilon_L + \varepsilon_H) \tag{3}$$

where ε_L and ε_H are energies of lowest unoccupied molecular orbital (LUMO) and highest occupied molecular orbital (HOMO), respectively. B3LYP/6-31G(d,p) level of theory was used to determine energies of HOMO and LUMO.

The evaluation is a crude approximation, and more reliable methods exist in the literature [76, 77]. Magnitudes of polarizability are very sensitive to the quality of basis set, and diffuse basis functions are more appropriate for its calculation [78]. Calculation of second order variation in energy with respect to electric fields (polarizability) for larger systems is computationally expensive; so we used data obtained from Hessian calculations carried out at B3LYP/6-31G(d,p) level of theory to determine exact tensorial components of polarizability α_{xx}, α_{yy} and α_{zz}. The mean value of polarizability is [78]:

$$\langle\alpha\rangle = \frac{1}{3}\left(\alpha_{xx} + \alpha_{yy} + \alpha_{zz}\right) \quad (4)$$

The stability of the species obtained in conceived pathways was verified using Principle of Maximum Hardness (PMH), i.e., molecular systems in equilibrium should be in a state of maximum hardness [79, 80] and minimum polarizability principle (MPP), i.e., natural direction of evolution of any system is toward a state of minimum polarizability [79, 81]. All quantum chemical computations were carried out using the Gaussian03 [62] suite of programs.

Results and discussion

We first discuss thermodynamic and kinetic aspects of the reaction energy pathways, followed by comments on the adequacy of the method and basis set used. The structural aspects connected to energetic trends shown by the reactants, reactive intermediates, transition states and products are discussed subsequently. Finally, NBO analysis and other reactivity parameters, and their relationship to the observed reactivity patterns are presented.

Thermodynamic and kinetic aspects

In the discussion below, the labels used for the different structures are described in Figs. 3 and 4. For each pathway, we consider different conformations of the reactant and take the lowest energy, electronic (ZPE) and free energy separately, as zero. The values of all other species are expressed relative to these values. Absolute values of zero point corrected electronic energy (E), enthalpy (H) and free energy (G) for different species in the concerted and stepwise pathways are shown in Tables S2–S3. Relative magnitudes of E (ΔE) and G (ΔG) for the species are shown in Tables S4–S5. Change in enthalpy, ΔH, and entropy term, TΔS, for formation of species obtained in various reactions are shown in Tables S6 and S7. Figure 5 shows the profiles of ΔE for reactions studied via the two different mechanisms considered.

The energy differences between the reactants (**1s**, **1c**, **2s** and **2c**) and corresponding products (**3**, **4**, **5** and **6**) indicate that intermolecular dimerization is favored and intramolecular cyclization is forbidden. Also, magnitudes of ΔE and ΔG for reactions leading to the cis dimer, **5**, −3.6 and −12.1 kcal/mol respectively; and that for trans dimer, **6**, −14.8 and −17.7 kcal/mol, respectively, indicate that the trans dimer is more stable than the cis dimer.

The role of kinetic control in the selectivity of dimer (inter) cyclization vs monomer (intra) cyclization was evaluated by comparing the energetic of the transition states along both the reaction pathways (concerted and stepwise). The plots shown in Fig. 5 indicate clearly that the dimer-cyclization is more favorable than the monomer-cyclization reaction.

Energy of activation, (ΔE) for **1sTS1**, **1sTS2**, **2sTS1** and **2sTS2** is 50.5, 45.1, 43.9 and 44.6 kcal/mol, respectively. The values for **1dsTS1** (**2dsTS1**), **1dsTS2a** (**2dsTS2a**), **1dsTS3a** (**2dsTS3a**) and **1dsTS4** (**2dsTS4**) are 38.3 (23.5),= 30.3 (24.6), 38.0 (20.4) and 31.5 (21.5) kcal/mol, respectively. Comparison of the magnitudes reveals that the barrier energy is relatively less for intermolecular cyclization. The relative energies of the activated complexes, **1dsTS2b/2dsTS2b** and **1dsTS3b/2dsTS3b** of reactions are greater than those of the corresponding geometries in the stepwise-a pathway, with a maximum difference of 19 kcal/mol (Fig. 5). Similar trends of the relative energies are exhibited by the intermediates connecting these two transition states (**1dsI2a** vs **1dsI2b** and **2dsI2a** vs **2dsI2b**). The energy differences between the two intermediates are found to be 33.9 and 21.4 kcal/mol in the **1Cy-di** and **2Cy-di** pathways, respectively. This is attributed to the presence of two highly unstable geminal diol moieties in the intermediates formed in the stepwise-b pathways. Further discussions on the stepwise path are based on stepwise-a unless otherwise noted.

Relative energies ΔE for activated complexes **1cTS** and **2cTS** are 51.5 and 47.2 kcal/mol, respectively. The magnitudes of **1dcTS1** and **1dcTS2** are 32.4, 33.0 kcal/mol and of **2dcTS1** and **2dcTS2** are 31.6, 26.9 kcal/mol, respectively. The concerted mechanism used for the cyclization reactions also reveals that intermolecular cyclization is kinetically favorable. Overall, the data indicate that kinetic control prefers intermolecular cyclization of the peptides rather than intramolecular cyclization.

The energy of activation of **1dcTS1** and **1dcTS2** is close to that of (**1dsTS1**, **1dsTS2a**) and (**1dsTS3a**, **1dsTS4**), respectively. This is in agreement with earlier reports of Oie et al. [48] and Jensen et al. [49], who have shown that stepwise and concerted mechanisms of uncatalyzed amide bond formation may compete since both involve comparable activation energies [82]. Comparison of ΔE for activated complexes in stepwise-a and concerted pathways of reaction **2Cy-di** indicates that the reaction paths are similar in terms of energy trends.

The ΔG profile of the reactions **1Cy-di** and **2Cy-di** shows that formation of linear dimers, **1dsI2a** and **2dsI2a**

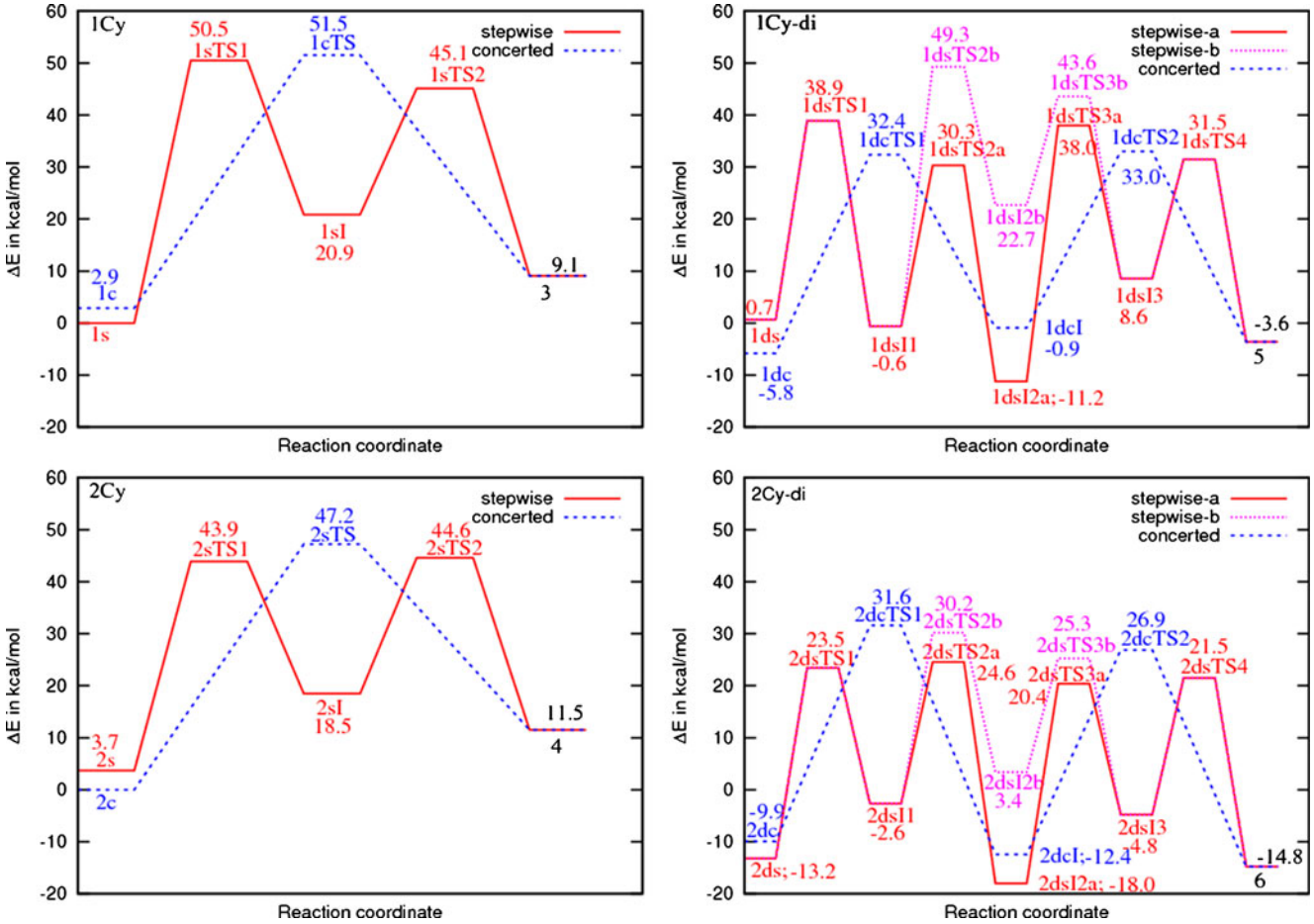

Fig. 5 Relative values of zero point corrected electronic energy (ΔE) of various structures obtained in stepwise and concerted mechanisms of reactions **1Cy, 2Cy** and stepwise-a, -b and concerted mechanisms of reactions, **1Cy-di, 2Cy-di**, in gas phase at B3LYP/6-31G(d,p) level of theory

is more favorable than that of **1dcI** and **2dcI**, respectively. Thus, the stepwise-a pathway for both reactions leading to the cis and trans dimers is the high yielding route. Rate constants (k) determined at various stages of reaction using Eq. 1 substantiate this result. Magnitudes of k calculated using $\Delta G^{\ddagger}$ of various TSs are shown in Table 1. In the stepwise-a mechanism of reaction **1Cy-di**, the formation of **1dsTS1** is the slowest (rate determining) step, and that of **1dsTS4** is fast. In the case of a concerted mechanism of reaction **1Cy-di**, formation of **1dcTS1** is the rate-determining step. Comparison of the energetics of activated complexes **1dsTS2a** and **1dcTS1** indicates that formation of the former is relatively faster (low value of $\Delta G^{\ddagger}$) than that of the latter. Both complexes are the immediate precursors of linear dimers (**1dsI2**/**1dcI**). This indicates that the yield of linear dimer is large when reaction **1Cy-di** uses the stepwise-a mechanism. Thus, this is the high yielding pathway for the cis dimer. A similar study on mechanisms leading to the trans dimer indicates that the formations of **2dsTS2a** and **2dcTS1** are the rate determining steps of the cyclization reaction using the stepwise-a and concerted mechanisms, respectively. Formation of **2dsTS2a** (the precursor of the linear dimer formed by **2**) is faster than **2dcTS1**. Thus, the yield of linear dimer **2dsI2a** is large, which in turn causes high yields of the trans dimer.

Single point energy (denoted ΔE_0 to distinguish from ΔE described earlier) calculations on all optimized geometries

Table 1 Rate constant (k) at various stages of reactions **1Cy-di** and **2Cy-di** using stepwise-a, -b and concerted mechanisms, determined at B3LYP/6-31G(d,p) level of theory

Structure	k (sec^{-1})	Structure	k (sec^{-1})
1dsTS1	3.776×10^{-28}	**2dsTS1**	5.990×10^{-18}
1dsTS2a	1.283×10^{-21}	**2dsTS2a**	7.891×10^{-19}
1dsTS2b	1.088×10^{-37}	**2dsTS2b**	2.748×10^{-25}
1dsTS3a	2.369×10^{-22}	**2dsTS3a**	2.170×10^{-10}
1dsTS3b	3.861×10^{-33}	**2dsTS3b**	1.205×10^{-22}
1dsTS4	4.097×10^{-16}	**2dsTS4**	5.617×10^{-11}
1dcTS1	5.177×10^{-23}	**2dcTS1**	3.118×10^{-23}
1dcTS2	1.310×10^{-18}	**2dcTS2**	8.578×10^{-15}

carried out on the array of basis sets mentioned in the methodology section also substantiated the observed energetic trends. The relative electronic energy (ΔE_0) profile for geometries at various stages of reactions, **1Cy** and **2Cy**, calculated using different basis sets is shown in Fig. 6. A similar energy profile obtained for reactions **1Cy-di** and **2Cy-di** is shown in Fig. 7. The magnitude of the energy change (ΔE_0) of all species is shown in Tables S8–S10. Changes in electronic energy are calculated with respect to the energy of stable reactant geometry (Fig. 6).

From Fig. 6, it can be seen that there is no significant change upon changing basis sets except that higher level calculations lead to marginally lower energies. More results and analysis on the effect of larger basis sets may be seen in Table S8. Reaction energies, ΔE_0, calculated using MP2/6-31G(d,p) level of theory showed reduced electronic energy barriers and formation energies of products when compared to that determined at B3LYP/6-31G(d,p) level of theory. This is due to improved accuracy in the description of correlation energies by the MP2 method [83, 84], and over-estimation of the dispersion interaction energy [85, 86].

In the case of reactions **1Cy-di** and **2Cy-di**, ΔE_0 of activated complexes is less than that in reactions **1Cy** and **2Cy**. This is seen generally for all DFT-B3LYP calculations using different basis sets. Change in the electronic energies of formation of **5** and **6** is also significantly less, close to zero. Indeed, at 6-311+G(d,p), 6-311++G(d,p), aug-cc-pVDZ, cc-pVTZ levels of basis set using B3LYP functional and at MP2/6-31G(d,p) level of theory, it is negative. These observations support our earlier predictions on the reactions based on B3LYP/6-31G(d,p) level of theory in the gas phase [45]. In summary, the qualitative trends of the energies of the intermediates, transition states and products in a given reaction pathway are independent of the quality of the basis set used. Similarly comparison of the trends across the different pathways yield similar conclusions.

Geometrical analysis

This section presents various geometric parameters and analyzes possible correlations with the energetics discussed above. We looked at torsion angle, ω, around all trans

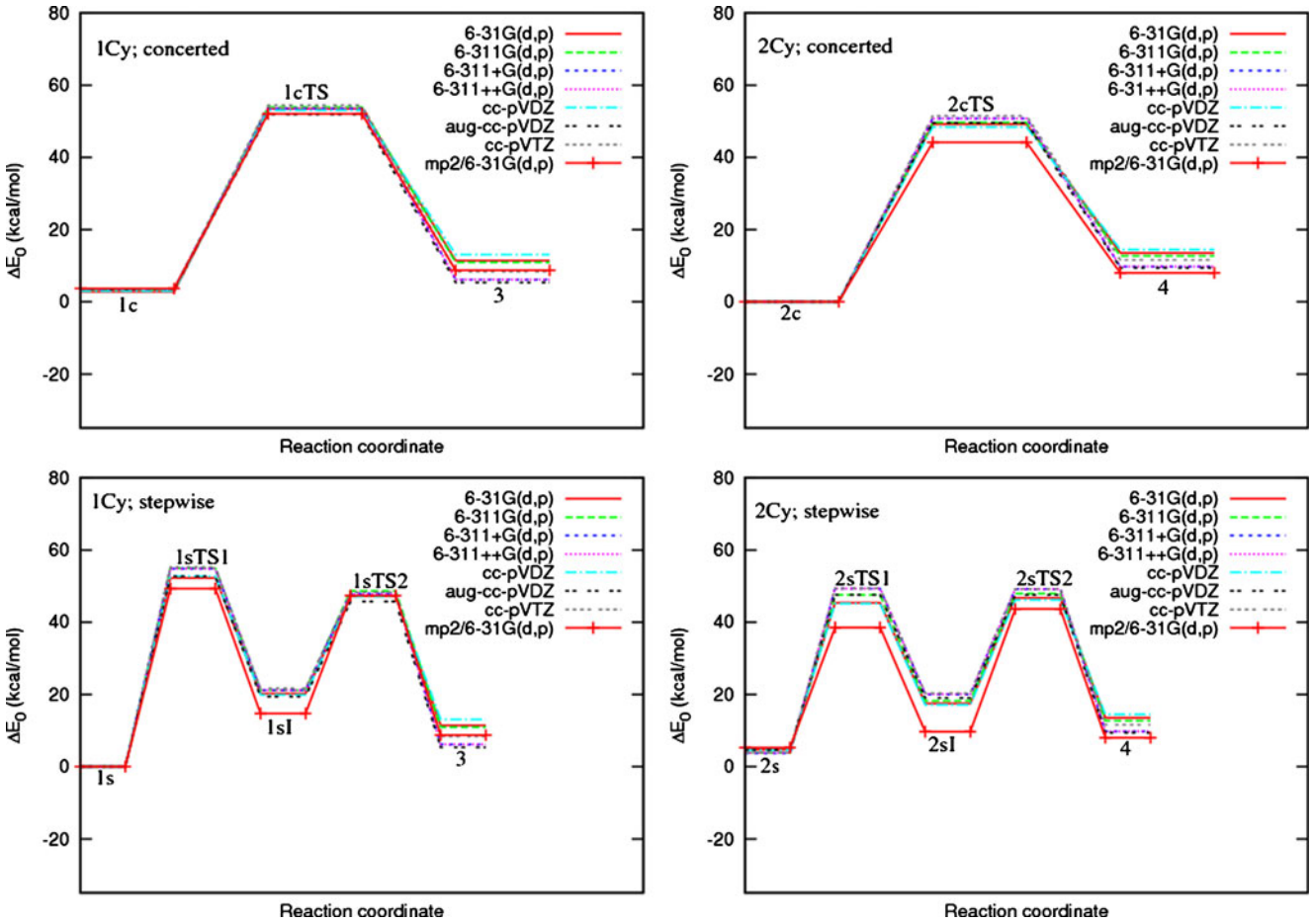

Fig. 6 Relative values of electronic energy (ΔE_0) of geometries obtained from concerted and stepwise mechanisms of reactions, **1Cy** and **2Cy** calculated at an array of basis sets, 6-31G(d,p), 6-311G(d,p), 6-311+G(d,p), 6-311++G(d,p), cc-pVDZ, aug-cc-pVDZ and cc-pVTZ using B3LYP functional and at MP2/6-31G(d,p) level of theory

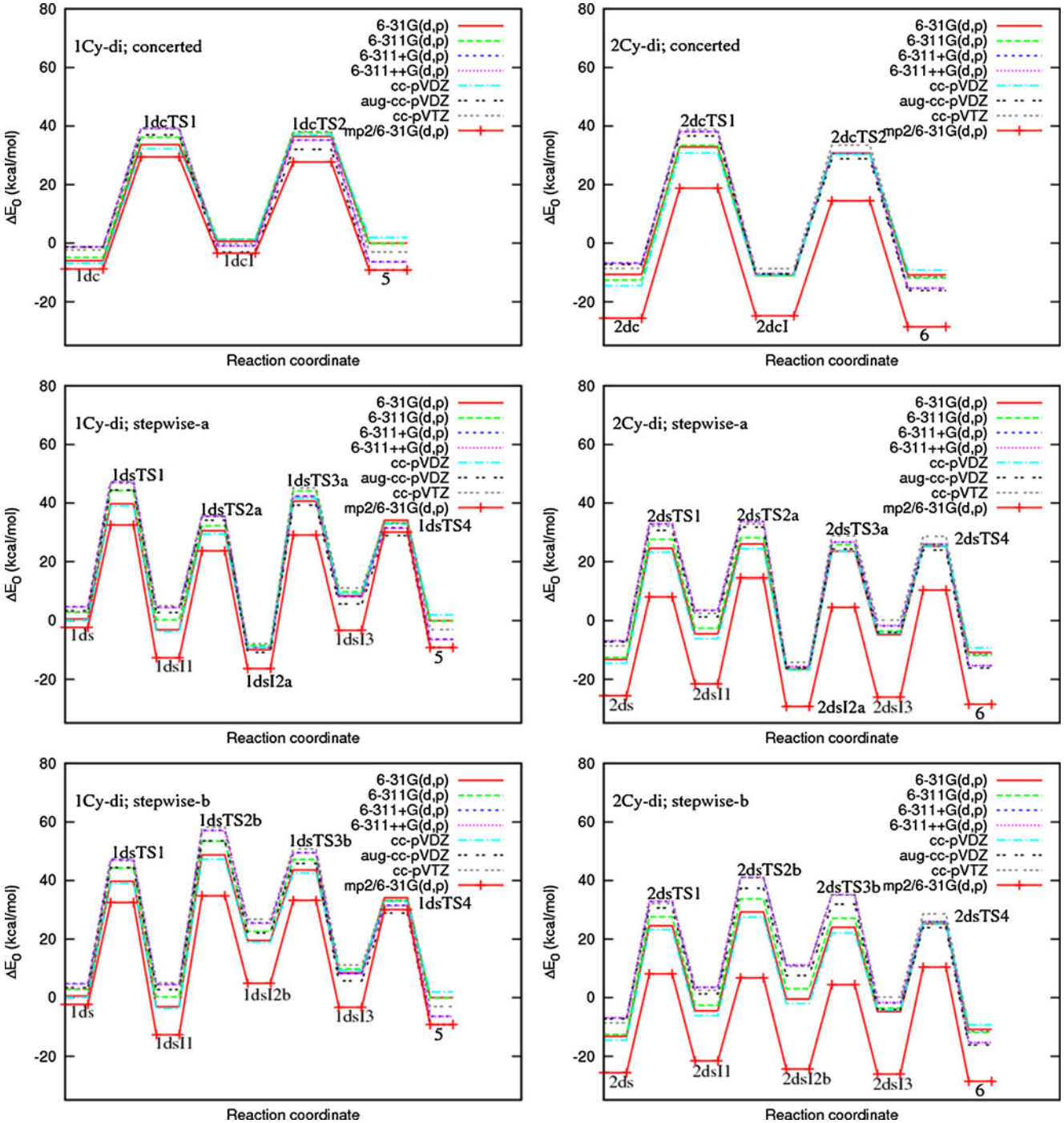

Fig. 7 Relative values of electronic energy (ΔE_0) of geometries obtained from concerted, stepwise-a and -b mechanisms of reactions, **1Cy-di** and **2Cy-di** calculated at an array of basis sets, 6-31G(d,p), 6-311G(d,p), 6-311+G(d,p), 6-311++G(d,p), cc-pVDZ, aug-cc-pVDZ and cc-pVTZ using B3LYP functional and at MP2/6-31G(d,p) level of theory

peptide bonds and other parameters in all geometries obtained from each of the reaction pathways. The atom numbering scheme shown in Fig. 8 is used for further analysis. Figures 9, 10 and S1–S4 show optimized geometries of species obtained in various mechanistic routes of reactions, **1Cy, 2Cy**, **1Cy-di** and **2Cy-di**.

Earlier studies on amide geometry and flexibility reported that the angle ω is between 166.0° and 194.0° in vacuum; and 168.0° and 192.0° in water at 300 K [67]. Rick and Cachau [68] also derived similar conclusions from a molecular dynamics study of protein structures. A survey of crystallographic data by MacArthur and Thornton [70] revealed that substantial

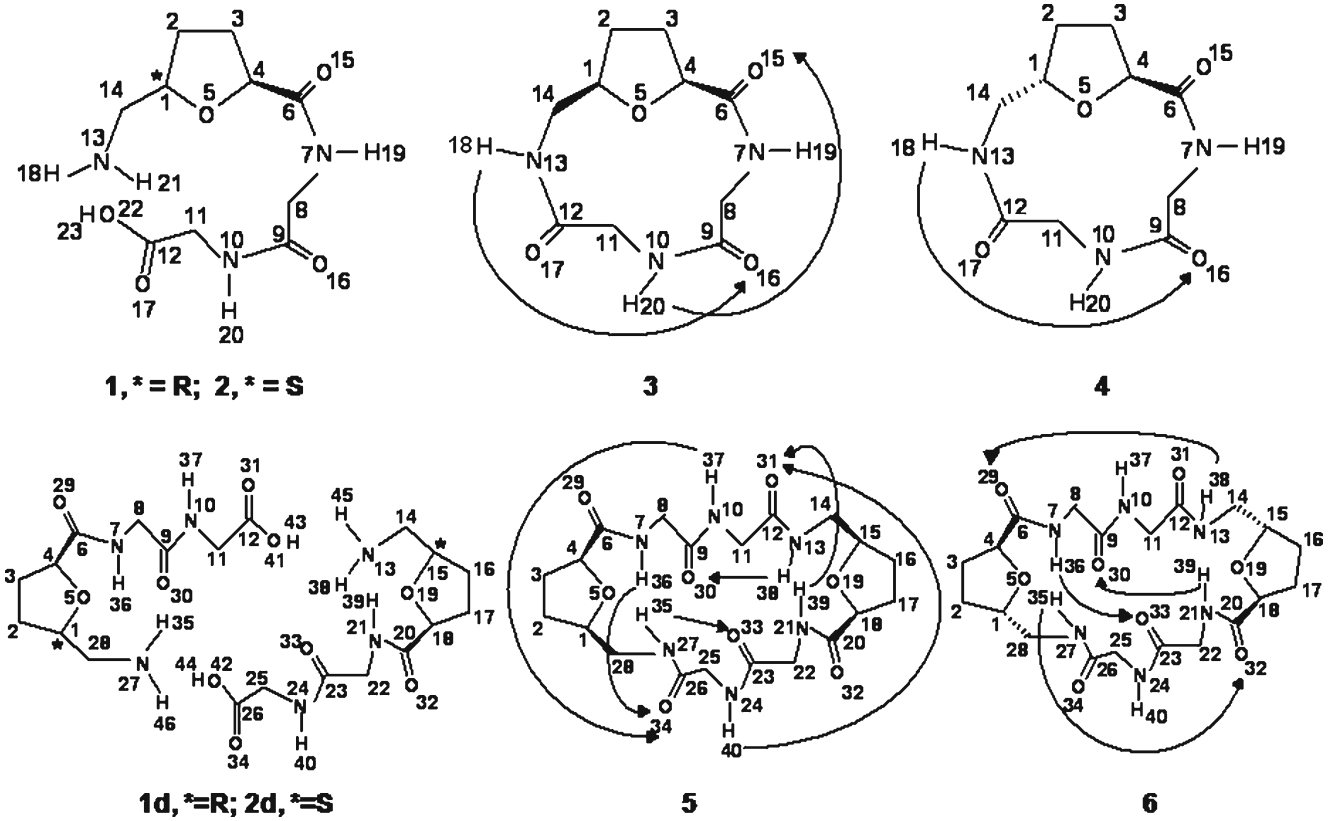

Fig. 8 **1**, **2** are reactant geometries for reactions **1Cy** and **2Cy**. **1d**, **2d** are reactant geometries for reactions **1Cy-di** and **2Cy-di**. Product geometries **3**, **4**, **5** and **6** are shown along with potential H-bonded interactions. The atom numbering scheme shown here refers to different geometries obtained in mechanistic study of the reactions **1Cy**, **2Cy** and **1Cy-di**, **2Cy-di**, respectively

distortion in planarity with a standard deviation in the angle up to 6° for the trans peptide can be tolerated. A computational analysis on NMA (N-methyl acetamide) carried out by Polavarapu et al. [71] also revealed that slightly nonplanar conformers ($\Delta\omega \sim 5$–°) represent true minima on the potential energy surface (PES) . Ramachandran showed that nonplanarity is an internal property of peptide bonds in cyclic peptides [72]. Using the results of these studies, we provide additional insights into torsional rotation around peptide bonds during intra and intermolecular cyclization of tripeptides.

Data for amide bond structure in intra products and their precursor geometries indicate that nonplanarity of the bond is beyond the allowed range of distribution of ω suggested by earlier studies (for details see Table S11). This is an important structural aspect responsible for observed large energy barriers and reaction energies in intramolecular cyclization reactions **1Cy** and **2Cy**.

On the other hand, peptide bond segments in geometries obtained in two reaction paths, **1Cy-di** and **2Cy-di** are planar and within the range suggested by earlier studies. The magnitudes of the angles are shown in Tables S12 and S13. Torsion angle ω_3 about a pair of peptide bonds C(12)–N(13) and C(26)–N(27) formed as a result of intermolecular cyclization of the linear tripeptides is −168.9° in **5** and −167.2° in **6**. The presence of such bonds is in accordance with Ramachandran's observation [72]. Formation of these bonds does not disturb the planarity of other existing peptide bonds. Additionally, the products **5** and **6** adopt "tennis ball seam-like" C_2 symmetric cyclic structures (Fig. 10). Thus intermolecular cyclization induces less strain in the molecular framework as compared to intramolecular cyclization, and hence is more facile.

To provide additional insights into structural features that show an impact on the cyclization reactions, we looked into the consequences of ω deformations. Distortion in the planarity of peptide bond changes the typical C–N, N–H and C=O bond lengths [67]. Amide bond lengths in all geometries obtained in reaction paths are shown in Table S14 (**1Cy** and **2Cy**) and in Tables S15–S17 (**1Cy-di** and **2Cy-di**). The C–N bond lengths are in the range of 1.36–1.37 Å and 1.36–1.38 Å, respectively, for **3** and **4** and in the range of 1.35–1.36 Å for inter products. Longer bonds in intra peptides indicate less delocalization of lone pair of electrons on nitrogen and the carbonyl group. The results further substantiate why cyclodimerization is favored over intramolecular cyclization of linear tripeptides.

While non-planarity of the peptide bond is a destabilizing factor, intramolecular hydrogen bonding interactions provide stability to the peptides [87]. The presence of stabilizing

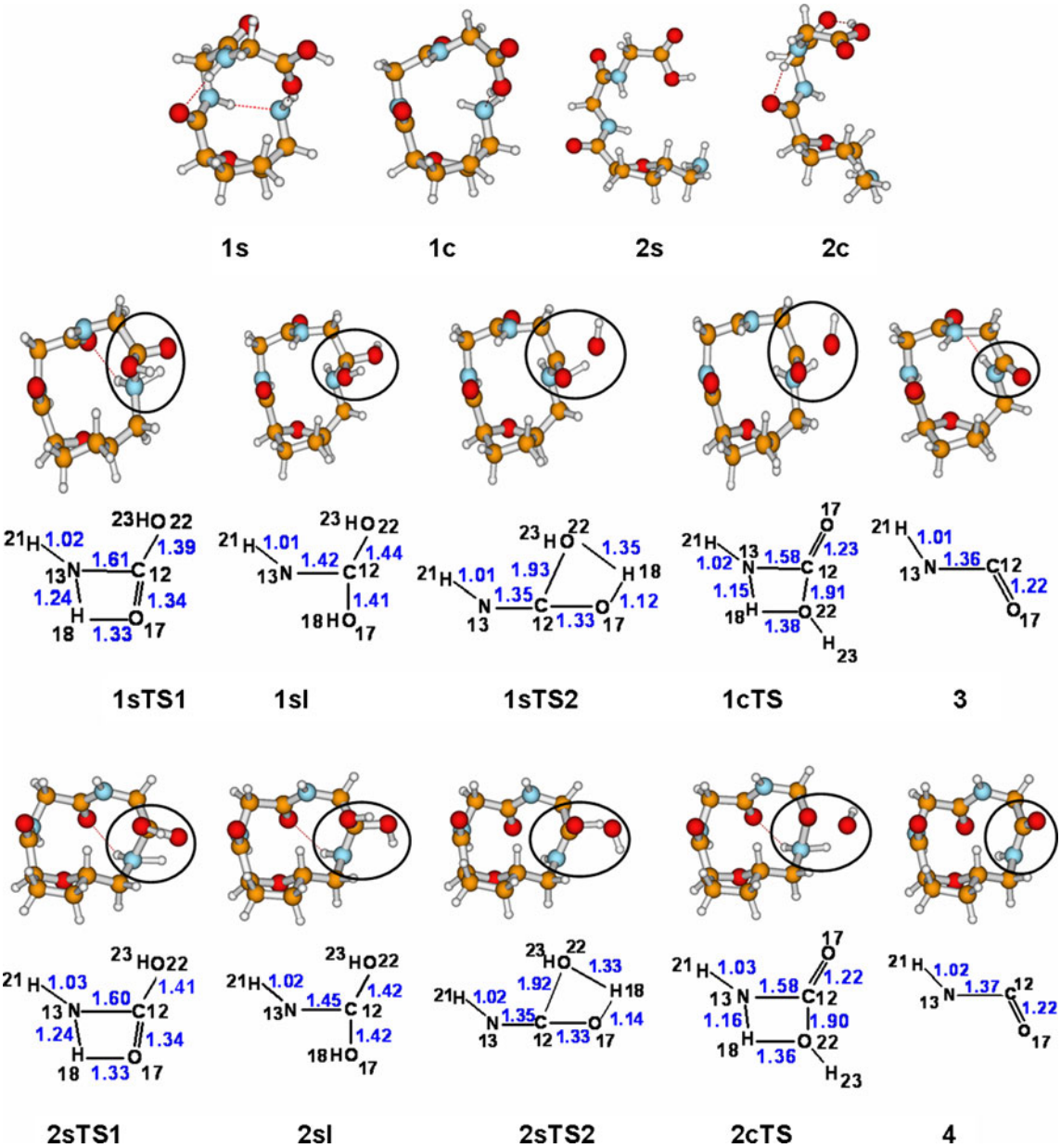

Fig. 9 Geometries of reactant, transition states and intermediates obtained from stepwise and concerted mechanisms of reactions **1Cy** and **2Cy**. The peptide bond segment is *circled*. Various bond lengths (in Å) of encircled geometry are shown below the respective structure

interactions in intermediates and transition states decreases the energy of activation of these reactions. We provide geometrical analysis of H-bonding interactions seen in all cyclic peptides, including those seen in their precursor geometries obtained from various reaction mechanisms applied for the reactions. Geometrical data for H-bonding interactions seen in geometries obtained from stepwise and concerted mechanisms of reactions, **1Cy** and **2Cy** are shown in Table S17–S20. Set of Tables S21–S26 and S27–S30 show geometrical parameters for all hydrogen bonding interactions in geometries obtained in reaction paths **1Cy-di** and **2Cy-di**, respectively.

Geometry of intra-TAA1 shows two C_7 hydrogen bonded cycles that form part of interactions N(13)-H(18)…O(16) and N(10)-H(20)…O(15). These are also observed in **1sTS1**, **1sI** and **1sTS2**; and **1cTS** of the reaction **1Cy**. While **1s** showed three H-bonds (Table S17), another conformation **1c** is associated with two such interactions (Table S18). This makes **1s** more stable than **1c** and also more stable when compared to **3**. Another cyclized product, intra-TAA2, shows one C_7 hydrogen bonded cycle (Fig. 8, Table S19). This is also observed in geometries **2sTS1**, **2sI**, **2sTS2** and **2cTS** of the reaction **2Cy**. Stable reactant geometry **2c** shows two H-bonding interactions (Table S20). The data indicate that the number of

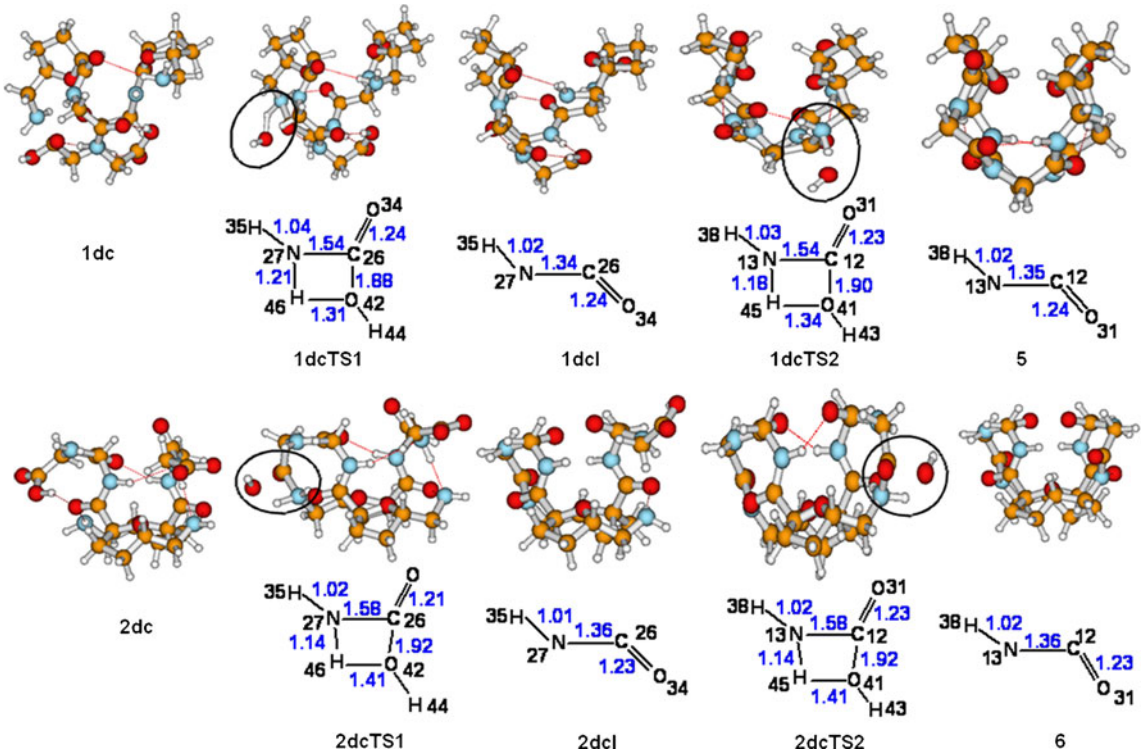

Fig. 10 Geometries of reactants, transition states and intermediates in the concerted mechanism of reaction **1Cy-di** (*top*) and **2Cy-di** (*bottom*). The peptide bond segment is *circled*. Various bond lengths (in Å) of encircled geometry are shown below the respective structure

stabilizing interactions in reactant geometries of the peptides is greater than that in intramolecularly cyclized products, thus explaining why reactions **1Cy** and **2Cy** are thermodynamically unfavorable.

The geometry of the cis dimer shows two sets of bifurcated H bonding interactions and two normal H-bonds (Fig. 8). A brief analysis of hydrogen bonding interactions associated with precursor geometries of the cis dimer obtained in stepwise a, -b and concerted pathways of **1Cy-di** is given below Table S26. Overall, the number of interactions associated with **1ds**; **1dsTS1**; **1dsI1**; **1dsTS2a, b; 1dsI2a, b; 1dsTS3a, b; 1dsI3** and **1dsTS4** is 4, 4, 5, 4(6), 6(6), 6(6), 6 and 6, respectively. The geometries **1dc**, **1dcTS1**, **1dcI**, **1dcTS2** of the reaction exhibit 6, 4, 5 and 6 hydrogen bonding interactions, respectively.

The geometry of the trans dimer shows four H-bonds (Fig. 8). Details of interactions associated with precursors of the trans dimer obtained in the stepwise-a, -b and concerted pathways are given below Table S30. In summary, the total number of interactions seen in geometries **2ds**; **2dsTS1**; **2dsI1**; **2dsTS2a, b; 2dsI2a, b; 2dsTS3a, b**; **2dsI3** and **2dsTS4** are 2, 4, 5, 6(4), 6(6), 6(6), 4 and 4, respectively. The concerted mechanism has 4, 3, 5 and 4 H-bonding interactions in **2dc**, **2dcTS1**, **2dcI** and **2dcTS2**, respectively.

The number of stabilizing hydrogen bonds either increases or does not change as intermolecular cyclization progresses. This is in contrast to the situation seen in intramolecular cyclization reactions. Additionally, the free energy barrier for intermolecular cyclization of TAA1 and TAA2 (Table S5) using the stepwise-a and concerted mechanisms is comparatively fewer, as the number of additional stabilizing interactions is greater than observed in the intramolecular cyclization reaction. The stepwise-b mechanism of both the intermolecular cyclization reactions involves **1dsTS2b/2dsTS2b** and **1dsTS3b / 2dsTS3b** with a sufficiently large number of stabilizing interactions. However, a large free energy of activation is seen for these transition states. This is due to the occurrence of geminal diol in these systems.

An important conformational aspect of the inter products is association of intramolecular hydrogen bonding interactions with protein secondary folding pattern-like structures. In the peptides containing tetrahydrofuran amino acids, the presence of such patterns is controlled by stereochemistry at the chiral centers 2 and 5 (Fig. 1) of the sugar ring, and the orientation of ring substitutions at the centers. At a given stereochemistry, possible orientations responsible for hydrogen bonded pseudo cycles in the cyclic products are determined by the torsion angles ζ and ρ. The details of these angles associated with various turn-like structures are given in Table 2. The angles ζ, ρ responsible for C_{10} and C_{13} cycles across both the THF rings in the cis dimer are −122.2° and 144.8°, respectively. Similarly, in the trans dimer, the 13-membered cycles are formed with the angles ζ=151.2° and ρ=121.0° at both rings. The magnitudes of these angles are

Table 2 Peptide torsion angles of hydrogen bonded cycles, Cx, measured from the N-terminal to C-terminal end of geometries **3**, **4**, **5** and **6** optimized in gas phase at B3LYP/6-31G(d,p) level of theory

Geometry	H-bonded cycle	cycle	ϕ (deg)	θ (deg)	ζ (deg)	ρ (deg)	ψ (deg)
3	N10-H20→O15	C_7	79.5	-	-	-	-86.3
	N13-H18→O16	C_7	-82.4	-	-	-	53.8
4	N13-H18→O16	C_7	-85.7	-	-	-	77.8
5	N7-H36→O34	C_{10}(ax,ax)	90.1	-60.4	-122.2	144.8	-37.5
	N21-H39→O31	C_{10}(ax,ax)	90.1	-60.4	-122.2	144.8	-37.5
	N10-H37→O34	C_{13}(ax,ax)	90.1	-60.4	-122.2	144.8	-37.5
			-88.7	-	-	-	-54.3
	N24-H40→O31	C_{13}(ax,ax)	90.1	-60.4	-122.2	144.8	-37.5
			-88.7	-	-	-	-54.3
	N13-H38→O30	C_7	-78.1	-	-	-	74.8
	N27-35→O33	C_7	-78.1	-	-	-	74.8
6	N13-H38→O29	C_{10}	-65.8	-	-	-	106.3
			68.4	-	-	-	23.6
	N27-H35→O32	C_{10}	-65.8	-	-	-	106.3
			68.4	-	-	-	23.6
	N7-H36→O33	C_{13}(ax,ax)	68.4	-	-	-	23.6
			78.9	60.0	151.2	121.0	-12.7
	N21-H39→O30	C_{13}(ax,ax)	68.4	-	-	-	23.6
			78.9	60.0	151.2	121.0	-12.7

almost reversed with the change in stereochemistry of TAA from (2S,5R) to (2S,5S). The ring substitutions are axially (ax) oriented at both 2, 5 positions of the rings in the cyclic dimers (see Methodology).

Another notable feature is that the relatively less planar peptide bond C(12)–N(13) and C(26)–N(27) in inter products (ω_3= −168.9° in **5**, ω_3=−167.2° in **6** for both peptide segments) facilitated the formation of a 7-membered H-bonded cycle (an inverse γ-turn type structures) in the cis dimer and a 10-membered H-bonding interaction (a β -turn type structure) in the trans dimer. Earlier conformational studies of cyclic pentapeptides (CPP) showed that at least one peptide unit needs to be distorted from planarity to form specific structural types such as β-,γ-turns [87]. The inter products formed by TAA1 and TAA2 are equivalent to cyclic hexapeptides. A deviation from planarity of the peptide bonds, and formation of an inverse γ-turn type structure shows a property similar to that exhibited by CPP.

NBO analysis

NBO analysis was performed to quantify the hydrogen bond interactions explained in the previous section using second order stabilization energies, $E^{(2)}$, corresponding to the interaction between lone pairs of H-acceptor atoms and the antibonding orbital of the H-donor bond. The results for reactions **1Cy** and **2Cy** are summarized in Tables S17–S20 and that of **1Cy-di** and **2Cy-di** are shown in Tables S21–S26 and S27–S30, respectively.

$E^{(2)}$ values corresponding to the hydrogen bonds observed in the reactant and product geometries were compared to evaluate the extent of their stabilization due to intramolecular interactions. The magnitude of stabilization energies of H-bonding interactions in the reactant geometries of **1Cy** and **2Cy** is relatively greater than that observed in the corresponding product geometries **3** and **4**, respectively. Reactant geometries exhibit strong hydrogen bonded interactions between the N- and C- terminal residues, e.g., N(7)–H(19)…N(13) ($E^{(2)}$=15.00 kcal/mol) in **1s**, O(22)–H(23)…N(13) ($E^{(2)}$=32.06 kcal/mol) in **1c** and O(22)–H(23)…O(16) ($E^{(2)}$=14.62 kcal/mol) in **2c**. Such strong interactions are also observed in reactant geometries of **5** and **6**. Intramolecular cyclization (formation of new peptide bond) eliminates the strong terminal group interactions and causes large distortion to the classic trans-planar peptide bonds. The deviation from the most stable planar peptide bond indicates that a reasonable strain is built up in the tripeptide due to intramolecular cyclization. On the other hand, intermolecular cyclization replaces terminal group interactions with peptide bonds but does not disturb the planarity of existing peptide bonds. This indicates that, unlike in the monomer cyclized product, the cyclic structures formed by the hexapeptide are large enough to accommodate planar peptide bonds with less or no distortion.

We compared stabilization energies of the common interactions in inter products and their corresponding reactant geometries. Magnitudes of $E^{(2)}$ for such interactions in reactant geometry, **1ds**/**1dc** obtained from all the three mechanisms is less than that seen in the product, **5**. Interestingly, in case of reaction path **2Cy-di**, using stepwise-a and -b mechanisms, $E^{(2)}$ for H-bonding interactions in the reactant is relatively larger than that observed in product

geometry. But, as discussed in previous section, the number of interactions in reactant geometry **2ds** is less than in the trans dimer (**6**). In summary, the stabilizing contribution due to hydrogen bonding indicates a preference for intermolecular cyclized products compared to intramolecular cyclized ones.

We observe a correlation among occupancy of the anti-bonding σ^*_{NH} orbital, $E^{(2)}$ and geometrical parameters of the N-H···O type of hydrogen bonding interactions seen in both products as well as its corresponding reactant geometry. For example, occupancy on σ^*_{NH} of interaction N(10)–H(20)···O (15) observed in minimum energy conformer of TAA1 (**1s**) is 0.038 and the value in intra-TAA1 is 0.026. In **1s** and intra-TAA1, the stabilization energy of the interaction is 2.39 and A and 0.99 kcal/mol, H···O bond distance is 2.02 Å and 2.28 Å and the bond angle of the interaction is 147.2° and 133.0°, respectively. The changes indicate that the stabilizing H-bond interaction becomes weaker during intramolecular cyclization of TAA1.

In case of the cis dimer (**5**) and its corresponding reactant geometry (**1ds**), we observed three common interactions, N (27)–H(35)···O(33), N(13)–H(38)…O(30) and N(21)–H (39)···O(31) (Tables S21, S23). For the first two interactions, the O···H bond distance and bond angle decrease, and occupancy and $E^{(2)}$ values increase; for the third interaction, the bond distance decreases, and bond angle, occupancy and $E^{(2)}$ increase. Similarly, the cis dimer and the reactant in the concerted reaction show three common interactions, N(27)–H(35)···O(33), N(13)–H(38)···O(30) and N(24) H(40)···O (31) (Table S23). Going from reactant to cis dimer, the first two interactions show an increase in occupancy of the anti-bonding orbital and stabilization energy as a result of the decrease in O···H bond distance and increase in bond angle; and the third interaction shows a slight increase in O···H bond distance and bond angle, and a slight decrease in the occupancy of σ^*_{NH} and value of $E^{(2)}$. A correlation between NBO parameters with at least one geometrical parameter that describes the H-bonding interaction is obtained. An important conclusion is that the stabilizing intramolecular interaction becomes stronger during intermolecular cyclization of TAA1.

The geometries of the trans dimer and intermediate **2ds** show two common interactions, N(7)–H(36)···O(33) and N (21)–H(39)···O(30) (Tables S25–S26). Going from reactant to product, stabilization energy and occupancy on σ^*_{NH} of both the interactions decrease as a result of increased O···H bond length and decreased bond angle. This correlation between changes in NBO and geometrical parameters of H-bonding interactions is as expected. We also observed two common interactions, N(27)–H(35)···O(32) and N (21)–H(39)···O(30) between the trans dimer and its corresponding reactant conformer obtained in the concerted mechanism (Table S30). The former interaction does not show the above-mentioned correlation, while the latter does. The observed decrease in the stabilization energy of the interaction does not favor formation of the trans dimer. As discussed in the previous section, the presence of a relatively large number of stabilizing interactions in the trans dimer compared to the reactant geometry further supports the feasibility of the reaction.

Hardness and polarizability profiles for the reactions

Descriptors such as chemical hardness and polarizability profiles of all species involved in the reactions were analyzed in order to provide additional insights into the preferential formation of cyclic peptide dimers. Chemical hardness (η), the energy separation between highest occupied molecular orbital (HOMO) and lowest unoccupied molecular orbital (LUMO), serve as measures of chemical stability [88, 89]. Hardness (η) indicates resistance to change in the electron distribution in a molecule. On the other hand, polarizability (α) measures the linear response of electron density in the presence of an infinitesimal electric field [90]. Studying the inverse relationship between hardness and polarizability for different chemical systems and situations is of great interest to computational chemists. Tables S31 and S32 show data for the energies of HOMO, LUMO, chemical potential, chemical hardness [derivative of chemical potential with respect to number of electrons (N_e) at constant external potential] and polarizabilities calculated for geometries obtained in stepwise and concerted mechanisms of the reactions **1Cy** - **2Cy** and **1Cy-di** - **2Cy-di**, respectively.

In all geometries obtained from both reaction mechanisms, the energy of HOMO (ε_H) does not change noticeably, and the energy of LUMO (ε_L) contributes the majority of the difference to the HOMO–LUMO energy gap. The energy separations ($\varepsilon_L - \varepsilon_H$), in **1s** and **1c** of **1Cy** are 6.19 and 6.47 eV, respectively. The corresponding value for **3** is 6.28 eV, indicating that the energy gap between HOMO and LUMO increases by 1.45% in a stepwise mechanism and decreases by 2.93% in the concerted mechanism of reaction **1Cy**. In the stepwise and concerted mechanisms of **2Cy** going from reactant to product, the energy gap changes by −1.25% and +1.44% respectively. Cyclic dimerization of **1** via stepwise and concerted mechanisms enhanced ($\varepsilon_L - \varepsilon_H$) by 15.04% and 13.58%, respectively. In the stepwise mechanism of reaction **2Cy-di**, the HOMO–LUMO separation decreases by 0.47%, and in the concerted pathway it increases by 5.14%. Comparing the fractional change in the HOMO–LUMO energy gap of reactant and product geometries in reactions leading to inter- and intra-molecular cyclization shows that paths corresponding to cyclic dimerization maximize the chemical hardness of the linear tripeptides.

Polarizability is used to understand the behavior of a system when changing the external field at a constant number of electrons. Magnitudes of polarizabilities of reactants and products are considered in order to verify the inverse

relationship between hardness and polarizability. We observed the simultaneous applicability of PMH and MPP for the considered geometries involved in the stepwise-a pathway of **1Cy-di** and those involved in concerted mechanisms of both the reactions **1Cy-di** and **2Cy-di**.

Conclusion

We have attempted to study the thermodynamic and kinetic control of monomer-cyclization vs dimer cyclization of linear tripeptides containing '2,5-cis'(2S,5R) and '2,5-trans' (2S,5S)-tetrahydrofuran amino acids. Thermodynamic data favor cyclic dimerization of the peptides in the gas phase. A kinetic study of the reactions shows that the activation energy barrier is relatively lower for intermolecular cyclization compared to intramolecular cyclization. We performed several calculations using a series of basis sets, and employing the MP2 method. Qualitatively similar results obtained from these calculations indicate that the trends presented and the conclusions derived are unlikely to change with change in basis set. Geometrical analysis of structures in the intramolecular cyclization reactions reveals that the observed activation free energy barrier is due to a large rotation around the amide bond, and a decrease in the number of stabilizing H-bonding interactions as the reaction proceeds. On the other hand, intermolecular cyclization does not disturb the planarity of existing peptide bonds. Nonplanarity in the peptide bonds of the intra products leads to longer C–N bonds than those in a typical peptide bond. Hydrogen bonding interactions observed in intra products resemble seven membered γ turns. The product cis dimer exhibits a host of secondary folding patterns like α-, β - and γ-turns whereas the trans dimer is associated with C_{10} (β -turn like) and C_{13} (α-turn like) cycles. NBO analysis of H-bonding interactions shows that the magnitudes of stabilization energies in intra products is less than that of the corresponding reactant geometries. Correlation between stabilization energy, occupancy of the antibonding orbital of the NH group, and the geometrical parameters of H-bonds is observed. The fractional change in chemical hardness in cyclic dimerization reactions for these peptides is large, indicating their preferential cyclodimerization. Simultaneous validity of maximum hardness and minimum polarizability principles is observed in the case of reactant and product geometries. This study motivates further thermodynamic and kinetic studies of solvent associated cyclization reactions of tripeptides, and enhances the scope to understand how a sugar ring induces turn-like structures associated with stabilizing intramolecular hydrogen bonds in peptides.

Acknowledgment We thank the Department of Science and Technology, New Delhi, Government of India for financial support (SR/S1/OC01/2007).

References

1. Gao X, Matsui H (2005) Peptide-based nanotubes and their applications in bionanotechnology. Adv Mater 17:20372050
2. Ulijn RV, Smith AM (2008) Designing peptide based nanomaterials. Chem Soc Rev 37:664675
3. Wipf P, Uto Y (2000) Total synthesis and revision of stereochemistry of the marine metabolite trunkamide A. J Org Chem 65:1037
4. Faulkner DJ (1999) Marine natural products. Nat Prod Rep 16:155
5. Wipf P (1998) In alkaloids: chemical and biological perspectives. Pelletier SW (ed) Pergamon, New York 187
6. Wipf P (1995) Synthetic studies of biologically active marine cyclopeptides. Chem Rev 95:2115
7. Pettit GR (1994) Marine animal and terrestrial plant anticancer constituents. Pure Appl Chem 66:2271
8. Davidson BS (1993) Ascidians: producers of amino acid-derived metabolites. Chem Rev 93:1771
9. Haberhauer G, Rominger F (2002) Synthesis of a new class of imidazole-based cyclic peptides. Tetrahedron Lett 43:6335
10. Roy RS, Gehring AM, Milne JC, Belshaw PJ, Walsh CT (1999) Thiazole and oxazole peptides: biosynthesis and molecular machinery. Nat Prod Rep 16:249
11. Wipf P, Fritch PC, Gieb SJ, Sefler AM (1998) Conformational studies and structure-activity analysis of Lissoclinamide 7 and related cyclopeptide alkaloids. J Am Chem Soc 120:4105
12. Li Y-M, Miline JC, Madison LL, Kollerand R, Walsh CT (1996) From peptide precursors to oxazole and thiazole containing peptide antibiotics: microcin B17 synthase. Science 274:1188
13. Foster MP, Concepcion GP, Caraan GB, Ireland CM (1992) Bistratamides C and D. Two new oxazole-containing cyclic hexapeptides isolated from a philippine lissoclinum bistratum ascidian. J Org Chem 57:6671
14. Graf von Roedern E, Kessler H (1994) A sugar amino acid as a novel peptidomimetic. Angew Chem Int Ed Engl 33:687–689
15. Gruner SAW, Locardi E, Lohof E, Kessler H (2002) Carbohydrate based mimetics in drug design: sugar amino acids and carbohydrate scaffolds. Chem Rev 102:491–514
16. Levine DP (2006) Vancomycin: a history. Clin Infect Dis 42: S5S12
17. Rüegger A, Kuhn M, Lichti H, Loosli H-R, Huguenin R, Quiquerez C, von Wartburg A (1976) Cyclosporin A, a peptide metabolite from trichoderma polysporum (Link ex Pers.) Rifai, with a remarkable immunosuppressive activity. Helv Chim Acta 59:10751092
18. Gause GF, Brazhnikova MG (1944) Gramicidin S and its use in the treatment of infected wounds. Nature 154:703
19. Jiang S, Li Z, Ding K, Roller P (2008) Recent progress of synthetic studies to peptide and peptidomimetic cyclization. Curr Org Chem 12:15021542
20. Haubner R, Gratias R, Diefenbach B, Goodman SL, Jonczyk A, Kessler H (1996) Structural and functional aspects of RGD containing cyclic pentapeptides as highly potent and selective integrin $\alpha_v\beta_3$ antagonists. J Am Chem Soc 118:74617472
21. Walensky LD, Kung AL, Escher I, Malia TJ, Barbuto S, Wright R, Wagner G, Verdine GL, Korsmeyer SJ (2004) Activation of apoptosis in vivo by a hydrocarbon-stapled BH3 helix. Science 305:14661470
22. Seebach D, Gardiner J (2008) β -Peptidic peptidomimetics. Acc Chem Res 41:13661375
23. Seebach D, Beck AK, Bierbaum D (2004) The world of beta- and gamma-peptides comprised of homologated proteinogenic amino acids and other components. J Chem Biodivers 1:1111–1239
24. Chakraborty TK, Srinivasu P, Tapadar S, Mohan BK (2005) Sugar amino acids in designing new molecules. Glycoconjugate J 22:83–93

25. Clark TD, Buehler LK, Ghadiri MR (1998) Self-assembling cyclic beta-3-peptide nanotubes as artificial transmembrane ion channels. J Am Chem Soc 120:651–656
26. van Maarseveen JH, Horne WS, Ghadiri MR (2005) Efficient route to C2 symmetric heterocyclic backbone modified cyclic peptides. Org Lett 7:4503–4506
27. Ghorai A, Gayen A, Kulsi G, Padmanaban E, Laskar A, Achari B, Mukhopadhyay C, Chattopadhyay P (2011) Simultaneous parallel and antiparallel self-assembly in a triazole/amide macro cycle conformationally homologous to d-, l–amino acid based cyclic peptides: NMR and molecular modeling study. Org Lett 13:5512–5515. doi:10.1021/ol2022356
28. Driggers EM, Hale SP, Lee J, Terrett NK (2008) Macrocycles for drug discovery an underexploited structural class. Nat Rev Drug Disc 7:608–624
29. White CJ, Yudin AK (2011) Contemporary strategies for peptide macrocyclization. Nat Chem 3:509–524
30. Jelokhani-Niaraki M, Kondejewski LH, Wheaton LC, Hodges RS (2009) Effect of ring size on conformation and biological activity of cyclic cationic antimicrobial peptides. J Med Chem 52:2090–2097
31. Bertram M, Hannam JS, Jolliffe KA, Gonzalez-Lopez de Turiso F, Pattenden G (1999) The synthesis of novel thiazole containing cyclic peptides via cyclooligomerization reactions. Synlett 1723–1726
32. Baldauf C, Günther R, Hofmann H-J (2004) δ -Peptides and δ amino acids as tools for peptide structure design-A theoretical study. J Org Chem 69:6214
33. Baldauf C, Günther R, Hofmann H-J (2006) Helix formation in α,γ-and β,γ-hybrid peptides: Theoretical insights into mimicry of α-andβ-peptides. J Org Chem 71:1200–1208
34. Martinek TA, Mándity IM, Fülöp L, Tóth GK, Vass E, Hollósi M, Forró E, Fülöp F (2006) Effects of the alternating backbone configuration on the secondary structure and self-assembly of β -peptides. J Am Chem Soc 128:13539–13544
35. Jockusch RA, Talbot FO, Rogers PS, Simone MI, Fleet GWJ, Simons JP (2006) Carbohydrate amino acids: the intrisic conformational preference for a β -turn-type structure in a carbopeptoid building block. J Am Chem Soc 128:16771–16777
36. Sandvoss LM, Carlson HA (2003) Conformational behavior fo β proline oligomers. J Am Chem Soc 125:15855–15862 C
37. Zhong H, Carlson HA (2006) Conformational studies of polyprolines. J Chem Theory Comput 2:342–353
38. D'hooghe M, Catak S, Stankovič S, Waroquier M, Kim Y, Ha HJ, Speybroeck VV, Kimpe ND (2010) Systematic study of Halide induced ring opening of 2-substituted aziridinium and theoretical rationalization of the reaction pathways. Eur J Org Chem 4920–4931
39. Chakraborty TK, Tapadar S, Kumar SK (2002) Cyclic trimer of 5-(aminomethyl)-2-furancarboxylic acid as a novel synthetic receptor for Carboxylate recognition. Tetrahedron Lett 43:1317–1320
40. Chakraborty TK, Srinivasu P, Bikshapathy E, Nagaraj R, Vairamani M, Kumar SK, Kunwar AC (2003) Cyclic homooligomers of furanoid sugar amino acids. J Org Chem 68:6257–6263
41. Chakraborty TK, Koley D, Rapolu R, Krishnakumari V, Nagaraj R, Kunwar AC (2008) Synthesis, conformational analysis and biological studies of cyclic cationic antimicrobial peptides containing sugar amino acids. J Org Chem 73:8731–8744
42. Pal S, Mitra K, Azmi S, Ghosh JK, Chakraborty TK (2011) Towards the synthesis of sugar amino acid containing antimicrobial noncytotoxic CAP conjugates with gold nanoparticles and their mechanistic study towards cell disruption. Org Biomol Chem 9:4806–4810
43. Leonard MS, Joullie MM (2002) Encyclopedia of reagents for organic synthesis. Wiley, New York
44. Kohn W, Becke AD, Parr RG (1996) Density functional theory of electronic structure. J Phys Chem 100:12974–12980
45. Kumar NVS, Sharma P, Singh H, Koley D, Roy S, Chakraborty TK (2010) Preferential mode of cyclization of tetrahydrofuran amino acids containing peptides: some theoretical insights. J Phys Org Chem 23:238–245
46. Chakraborty TK, Roy S, Koley D, Dutta SK, Kunwar AC (2006) Conformational analysis of some C_2-Symmetric cyclic peptides containing tetrahydrofuran amino acids. J Org Chem 71:6240–6243
47. Joullié MM, Lassen KM (2010) Evolution of amide bond formation. ARKIVOC viii:189–250
48. Oie T, Loew GH, Burt SK, Binkley JS, MacElroy RD (1982) Quantum chemical studies of a model for peptide bond formation: formation of formamide and water from ammonia and formic acid. J Am Chem Soc 104:6169–6174
49. Jensen JH, Baldridge KK, Gordon MS (1992) Uncatalyzed peptide bond formation in the gas phase. J Phys Chem 96:8340
50. Krug JP, Popelier PLA, Bader RFW (1992) Theoretical study of neutral and of acid and base-promoted hydrolysis of formamide. J Phys Chem 96:7604–7616
51. Antonczak S, Ruiz-López MF, Rivail JL (1994) Ab initio analysis of water-assisted reaction mechanisms in amide hydrolysis. J Am Chem Soc 116:3912–3921
52. Pan B, Ricci MS, Trout BL (2011) A molecular mechanism of hydrolysis of peptide bonds at neutral pH using a model compound. J Phys Chem B 115:5958–5970
53. Sybyl version7.2, c.o.http://www.tripos.com
54. Gaurrand S, Desjardins S, Meyer C, Bonnet P, Argoullon JM, Oulyadi H, Guillemont J (2006) Conformational analysis of r207910, a new drug candidate for the treatment of tuberculosis, by a combined NMR and molecular modeling approach. Chem Biol Drug Des 68:77–84
55. Becke AD (1988) Density-functional exchange energy approximation with correct asymptotic behavior. Phys Rev A 38:3098–3100
56. Lee C, Yang W, Parr RG (1988) Development of the Colle-Salvetti correlation-energy formula into a functional of the electron density. Phys Rev B 37:785–789
57. Becke AD (1993) Density-functional thermochemistry. III. The role of exact exchange. J Chem Phys 98:5648–5652
58. Hehre WJ, Radom L, Schleyer PVR, Pople JA (1986) Ab initio molecular orbital theory. Wiley-Interscience, New York
59. Guimarães CRW, Repasky MP, Chandrasekhar J, Tirado-Rives J, Jorgensen WL (2003) Contributions of conformational compression and preferential transition state stabilization to the rate enhancement by chorismate mutase. J Am Chem Soc 125:6892–6899
60. Zhang X, Bruice TC (2007) Diels-alder ribozyme catalysis: a computational approach. J Am Chem Soc 129:1001–1007
61. Gorb L, Asensio A, Tuñón I, Ruiz-López MF (2005) The mechanism of formamide hydrolysis in water from ab initio claculations and simulations. Chem Eur J 11:6743–6753
62. Frisch MJ et al (2003) Gaussian03, revision B.05; Gaussian, Pittsburg, PA
63. Laidler KJ (1987) Chemical kinetics, 3rd edn. Harper & Row, New York
64. Chiodo SG, Leopoldini M, Russo N, Toscano M (2010) The inactivation of lipid peroxide radical by quercetin A. Theor Insight 12:7662–7670
65. Černý J, Hobza P (2007) Non-covalent interactions in biomacro molecules. Phys Chem Chem Phys 9:5291–5302
66. Chalupský J, Vondrášek J, Špirko V (2008) Quasiplanarity of the peptide bond. J Phys Chem A 112:693–699
67. Bednárová L, Maloň P, Bouř P (2007) Spectroscopic properties of the nonplanar amide group: a computational study. Chirality 19:775–786

68. Rick SW, Cachau RE (2000) The nonplanarity of the peptide group: molecular dynamics simulations with a polarizable two-state model for the peptide bond. J Chem Phys 112:5230
69. Ramek M, Yu C-H, Sakon J, Schäfer L (2000) Ab initio study of the conformational dependence of the nonplanarity of the peptide group. J Phys Chem A 104:9636–9645
70. MacArthur MW, Thornton JM (1996) Deviations from planarity of the peptide bond in peptides and proteins. J Mol Biol 264(5):1180–1195
71. Polavarapu PL, Deng ZY, Ewig CS (1994) Vibrational properties of the peptide group: achiral and chiral conformers of N-methylacetamide. J Phys Chem 98:9919–9930
72. Ramachandran GN (1968) Need for nonplanar peptide units in polypeptide chains. Biopolymers 6:1494–1496
73. Chakraborty TK, Kumar NVS, Roy S, Dutta SK, Kunwar AC, Sridhar B, Singh H (2011) Stereochemical control in the structures of linear δ, α-hybrid tripeptides containing tetrahydrofuran amino acids. J Phys Org Chem 24:720–731
74. Read AE, Weinstock RB, Weinhold F (1985) Natural population analysis. J Chem Phys 83:735
75. Ayers PW, Parr RG, Pearson RG (2006) Elucidating the hard/soft acid/base principle: a perspective based on half-reactions. J Chem Phys 124:194107
76. Mineva T, Sicilia E, Russo N (1998) Density-Functional approach to hardness evaluation and its use in the study of the maximum hardness principle. J Am Chem Soc 120:9053–9058
77. Luca GD, Sicilia E, Russo N, Mineva T (2002) On the hardness evaluation in solvent for neutral and charged systems. J Am Chem Soc 124:1494–1499
78. Fuentealba P, Simón-Manso Y, Chattaraj PK (2000) Molecular electronic excitations and the minimum polarizability principle. J Phys Chem A 104:3185–3187
79. Pearson RG (1997) Chemical hardness: applications from molecules to solids. Wiley-VCH, Weinheim
80. Datta D (1992) "Hardness profile" of a reaction path. J Phys Chem 96:2409
81. Parr RG, Yang W (1989) Density functional theory of atoms and molecules. Oxford University Press, New York
82. Chalmet S, Harb W, Ruiz-López MF (2001) Computer simulation of amide bond formation in aqueous solution. J Phys Chem A 105:11574–11581
83. Jensen F (2007) Introduction to computational chemistry, 2nd edn. Wiley, London
84. Koch W, Holthausen MC (2001) A chemist's guide to density functional theory. Wiley-VCH, New York
85. Jurečka P, Šponer J, Černý J, Hobza P (2006) Benchmark database of accurate (MP2 and CCSD(T) complete basis set limit) interaction energies of small model complexes, DNA base pairs, and amino acid pairs. Phys Chem Chem Phys 8:1985–1993
86. Cybulski SM, Lytle ML (2007) The origin of deficiency of the supermolecule second-order Møller-Plesset approach for evaluating interaction energies. J Chem Phys 127:141102
87. Nagarajam HA, Ramakrishnan C (1995) Stereochemical studies on cyclic peptides: detailed energy minimization studies on hydrogen bonded all-trans cyclic pentapeptide backbones. J Biosci 20:591–611
88. Hess BA, Schaad LJ (1971) Hueckel molecular orbital π resonance energies. The benzenoid hydrocarbons. J Am Chem Soc 93:2413–2416
89. Pearson RG (1988) Electronic spectra and chemical reactivity. J Am Chem Soc 110:2092–2097
90. Foresman JB, leen Frisch Æ (1996) exploring chemistry with electronic structure methods 2nd edn. Gaussian, Pittsburgh, PA